ISSN 1067-8212, Russian Journal of Non-Ferrous Metals, 2015, Vol. 56, No. 1, pp. 44–51. © Allerton Press, Inc., 2015.
Original Russian Text © B.B. Straumal, A.A. Mazilkin, X. Sauvage, R.Z. Valiev, A.B. Straumal, A.M. Gusak, 2014, published in Izvestiya VUZ. Tsvetnaya Metallurgiya, 2014, No. 6, pp. 44–50.

PHYSICAL METALLURGY AND HEAT TREATMENT

Pseudopartial Wetting of Grain Boundaries in Severely Deformed Al–Zn Alloys

B. B. Straumal[a, b, c, *], A. A. Mazilkin[a, b, **], X. Sauvage[d, *], R. Z. Valiev[e, ****], A. B. Straumal[a, b, *****], and A. M. Gusak[f, ******]**

[a] *Laboratory of Hybrid Nanomaterials, National University of Science and Technology "MISiS", Leninskii pr. 4, Moscow, 119049 Russia*

[b] *Institute of Solid State Physics, Russian Academy of Sciences, ul. Akademika Osip'yana 2, Chernogolovka, Moscow region, 142432 Russia*

[c] *Karlsruher Institut für Technologie, Institut für Nanotechnologie, Hermann-von-Helmholtz Platz 1, 76344 Eggenstein-Leopoldshafen, Germany*

[d] *Université de Rouen, CNRS, UMR 6634, Avenue de l'Université, BP 12–76801 St-Etienne-du-Rouvray, France*

[e] *Ufa State Aviation Technical University, K. Marx str. 12, Ufa, 450000 Russia*

[f] *Cherkasy National University, Shevchenko bulv. 81, Cherkasy 18027 Ukraine*

**e-mail: straumal@issp.ac.ru*

***e-mail: mazilkin@issp.ac.ru*

****e-mail: xavier.sauvage@univ-rouen.fr*

*****e-mail: rzvaliev@mail.rb.ru*

******e-mail: AStraumal@misis.ru*

*******e-mail: gusak@cdu.edu.ua*

Abstract—After severe plastic deformation by the high-pressure torsion, Al–Zn alloys have three various classes of Al/Al grain boundaries (GBs) wetted with a second zinc-rich phase. Completely wetted Al/Al GBs are coated with the layer of a zinc-rich phase more than 30 nm thick. Partially (incompletely) wetted Al/Al GBs contact particles of the zinc-rich phase with a contact angle >60°, but contain no measurable zinc concentration. Pseudopartially wetted Al/Al GBs also contact Zn particles with a contact angle >60°. However, they have a thin interlayer of the zinc-rich phase with a uniform thickness of 2–4 nm, the presence of which explains the unusually high ductility of Al–Zn alloys after high-pressure torsion.

Keywords: grain boundaries, severe plastic deformation, high-pressure torsion, wetting

DOI: 10.3103/S1067821215010198

INTRODUCTION

Wetting of free surfaces and inner interfaces is important not only for various technologies (oil extraction, soldering, welding, sintering, water drainage from roads, effective deposition of pesticides on plant leaves, etc.) but is also associated with discovering new physical phenomena [1–9]. Partial or incomplete (Figs. 1a, 1b) and complete (Figs. 1c, 1d) wetting (IW and CW) of the surface and/or internal interfaces are distinguished. If there is a small amount of liquid with CW and the area of the surface or the grain boundary (GB) is large, then liquid propagates laterally until both solid grains or solid substrate and gas would start to interact with one another through the liquid layer. The latter forms a "pancake" with thickness $e_s \approx 2$–5 nm in this case [1, 10]:

$$e_s = [A/(4\pi S)]^{1/2}. \quad (1)$$

Here, $S = \sigma_{sg} - \sigma_{sl} - \sigma_{lg}$ is the spreading coefficient over a dry solid surface, where σ_{sg}, σ_{sl}, and σ_{lg} are free energies of solid/gas, solid/liquid, and liquid/gas interfaces; A is the Hamaker constant [11]. In the case of complete wetting, $A > 0$ and $S > 0$ [10].

In most cases, the immediate transition between partial (incomplete) wetting (see phase diagram in Fig. 1g proposed in [2]) and complete wetting, for example, upon heating [12, 13] or rarefaction [14] is observed.

However, the state of pseudopartial wetting (PPW), which is arranged in the phase diagram between IW and CW (see Fig. 1g), is sometimes observed. In this case, contact angle $\theta > 0$ and a liquid droplet does not spread over the substrate; however, a thin (several nanometers thick) precursor film which separates the substrate and gas occurs around it (see Fig. 1e). Such a film is similar to a quasi-liquid "pancake" in the case of CW and a deficit of the liquid phase (see above, as well as [15, 16]). Pseudopartial wetting was observed for the first time on the of free surface [2, 17]; it also occurs on the GB [3, 4].

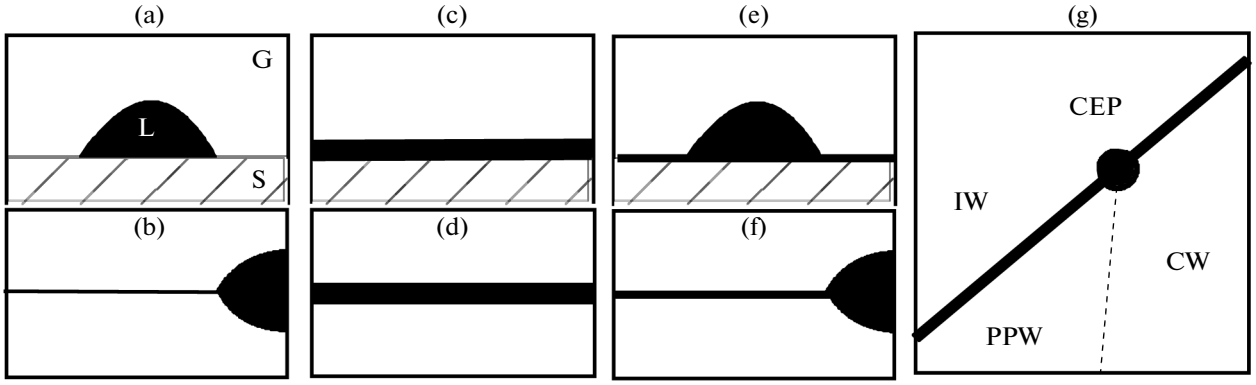

Fig. 1. Schematic diagrams illustrating the wetting of free surfaces and GBs. (a, b) Incomplete wetting of (a) the of free surface (L is the liquid phase, S is the solid phase, and G is the gas phase) and (b) GBs; (c, d) complete wetting of (c) the surface and (d) GBs; (e, f) pseudopartial wetting of (e) the surface and (f) GBs; and (g) mutual arrangement of wetting transformations IW ↔ PPW ↔ CW ↔ IW [2] (CEP is the critical end point, the thick solid line denotes the first-order wetting transition, and the thin dashed line is the second-order (continuous) transition).

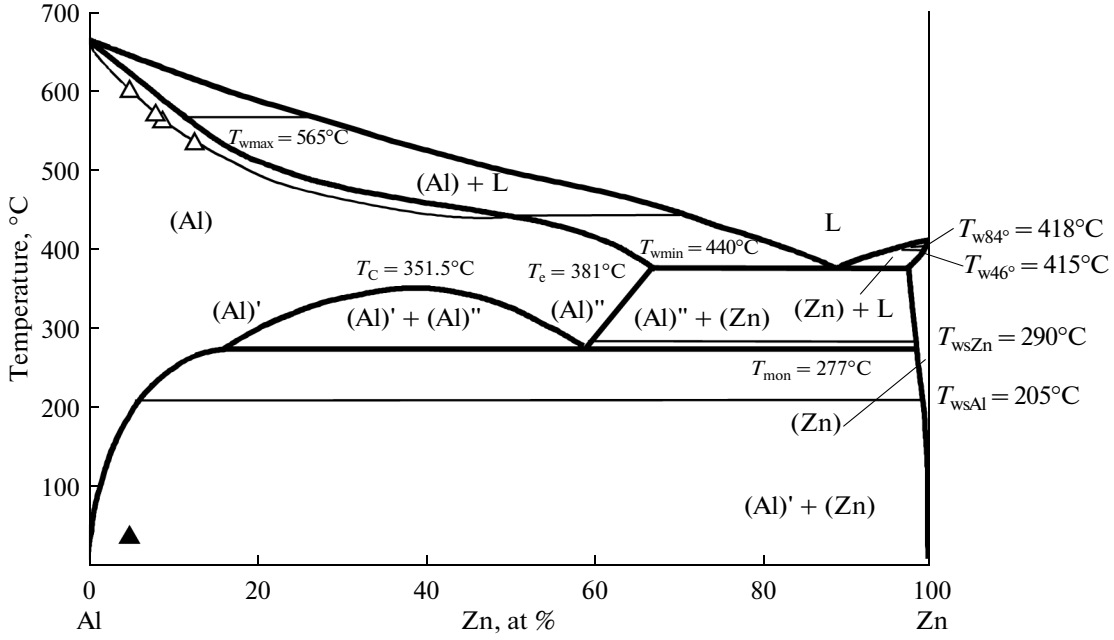

Fig. 2. Al–Zn phase diagram plotted using the data [13, 19–22, 24]. Thick lines corresponds to bulk phase transformations [36] and thin lines correspond to phase transformations at GBs. Bright triangles denote TEM and DSC data for the GB prewetting line and a dark triangle denotes the HPT conditions in this article. T_w and T_{ws} are temperatures of wetting phase transitions by the liquid phase and second solid phase, correspondingly; T_c, T_e, and T_{mon} are critical, eutectic, and monotectic temperatures, respectively.

The presence of thin intergrain interlayers for most GBs and a simultaneous absence of thick wetting melt layers separating the matrix grains can be extremely important to monitor the properties of polycrystalline materials and should be investigated in detail. This is the goal of our study.

The Al–Zn system is a good object for such investigations (Fig. 2). In Al–Zn alloys various GB wetting transitions both of the first and second orders [13] both by the liquid phase [12–14, 18] and the second solid phase [19, 20] take place. Thin quasi-liquid interlayers at GBs and GB triple junctions were observed using transmission electron microscopy (TEM) [17, 21] and differential scanning calorimetry [21, 22]. Thus, it is reasonable to seek the PPW of the GB by the second solid phase just in these materials.

Unfortunately, the diffusion in Al–Zn alloys is extremely slow below 200°C, and we could not investigate the wetting phenomena using usual thermal annealing for an acceptable period (<6 months).

Therefore, instead of prolonged annealings, we used severe plastic deformation (SPD) by high-pressure torsion (HPT) to produce ultra-fine-grain polycrystals at room temperature.

It was shown in our previous article [21] that the contact angle between Zn grains and Al/Al GBs, which is seen in usual TEM micrographs after the HPT, was about 60° and, consequently, it was far from zero. On the other hand, ultrafine-grained Al–30 wt % Zn alloys possess unusually high room-temperature ductility after the HPT [23]. We assumed that zinc-rich interlayers along the boundaries will promote mutual sliding along Al/Al GBs as a peculiar lubricant.

EXPERIMENTAL

The Al–10 wt % Zn alloy was fabricated from high-purity components (99.999% Al and 99.9995% Zn) using vacuum induction melting. Then it was cast in vacuum into water-cooled copper crucibles with an inner diameter of 10 mm. The deformation was performed at room temperature using the HPT process. Casts were cut into discs about 0.7 mm thick and 10 mm in diameter. Each disc was placed between two steel anvils. The applied pressure was 6 GPa, and the strain rate was 1 rpm. The deformation was determined by the number of anvil rotations $N = 5$.

Analytical TEM has been performed with a ARM200F JEOL microscope operating at 200 kV. High-angle annular dark-field images (HAADFs) were recorded in a scanning mode (STEM) using a probe size of 0.2 nm with a convergence angle of 34 mrad and collection angles in the range of 80 to 300 mrad.

RESULTS

Similarly to [24], the supersaturated solid solution in cast alloys decomposed after the HPT almost completely. The average grain size in aluminum decreased from 500 μm to 800 μm in the course of deformation, while for Zn particles it decreased from 5 μm to 200 nm. Figure 3a shows the HAADF micrograph, where the contrast is associated with the average local atomic number.

Thus, zinc-rich zones look bright, while dark segments correspond to aluminum. A white zinc grain is seen in the lower micrograph part. The Al/Al grain boundary, which ranges from the lower to the upper part of the photograph, is also observed. The arrow in the upper part shows a segment of GB which is completely wetted by the Zn-rich phase.

The intensity profile of the HAADF signal across the Al/Al GB (see Fig. 3b) shows that the thickness of the Zn-rich layer is about 30 nm (the elongated white rectangle in Fig. 3a shows the profile position). Figures 3c and 3d show electron diffraction patterns from local segments (LSEs) from left 1 and right 2 aluminum grains (Fig. 3a), respectively, which allows us to determine the normal to sample planes [114] and [547]. This fact means that the GB is asymmetric.

Figure 4a represents the bright-field image, which shows zinc grain (dark) in the right part and incompletely wetted Al/Al GB (it is started in the left lower angle of the photograph and is elongated to the right upwards). The contact angle between the Zn particle and Al/Al GB is about 115°. The intensity of the HAADF signal in the profile perpendicular to this boundary does not manifest its enrichment with zinc. This case corresponds to incomplete wetting of the Al/Al GB with the zinc-rich phase. Electron diffraction patterns from local segments of the upper and lower Al grains are presented in Figs. 4c and 4d. Corresponding normals to the sample plane are defined as [001] and [114].

A zinc grain (dark) and two pseudopartially wetted Al/Al GBs (they are directed from the middle upwards to the left and to the right) are observed in the bright-field STEM image (Fig. 5a). Two corresponding HAADF images recorded in the Z-contrast mode are presented in Figs. 5b and 5c. Contact angles between the Zn particle and Al/Al GBs are about 110° (left GB) and 60° (right GB). These boundaries are clearly seen in the image as bright lines, which points to the local enrichment with zinc. Intensity profiles of the HAADF signal at the left and right Al/Al GBs in Figs. 5d and 5e contain high but narrow maxima. These profiles show zinc-rich layers at the GB with a thickness of 1–2 nm.

Electron diffraction patterns from segments of the left, middle, and right aluminum grains are presented in Figs. 5f–5h. Corresponding normals to the sample plane are [110], [111], and [114]. This means that both Al/Al GBs are asymmetric.

Figure 6 shows a high-resolution TEM micrographs of one of pseudopartially wetted Al/Al GBs. Both Al grains remain crystalline, and there are no amorphous layers at the GB. Approximately 20–30% of GBs observed in the samples are PPW.

DISCUSSION

We should primarily note that the state of the material after the HPT (both of bulk and GB phases) is not equilibrium at the HPT pressure and temperature. In our case, it corresponds to the steady state, which is attained in Al–Zn alloys after ~1 rotation of anvils [24]. Therefore, it would be incorrect to affirm that the HPT application is equivalent to an increase in the annealing duration. The steady state during the SPD is usually observed upon attaining a definite degree of deformation. The grain size, strength, hardness, long-range order parameter, composition of phases, etc., stop varying with an increase in deformation in this case (i.e., the number of passages during the

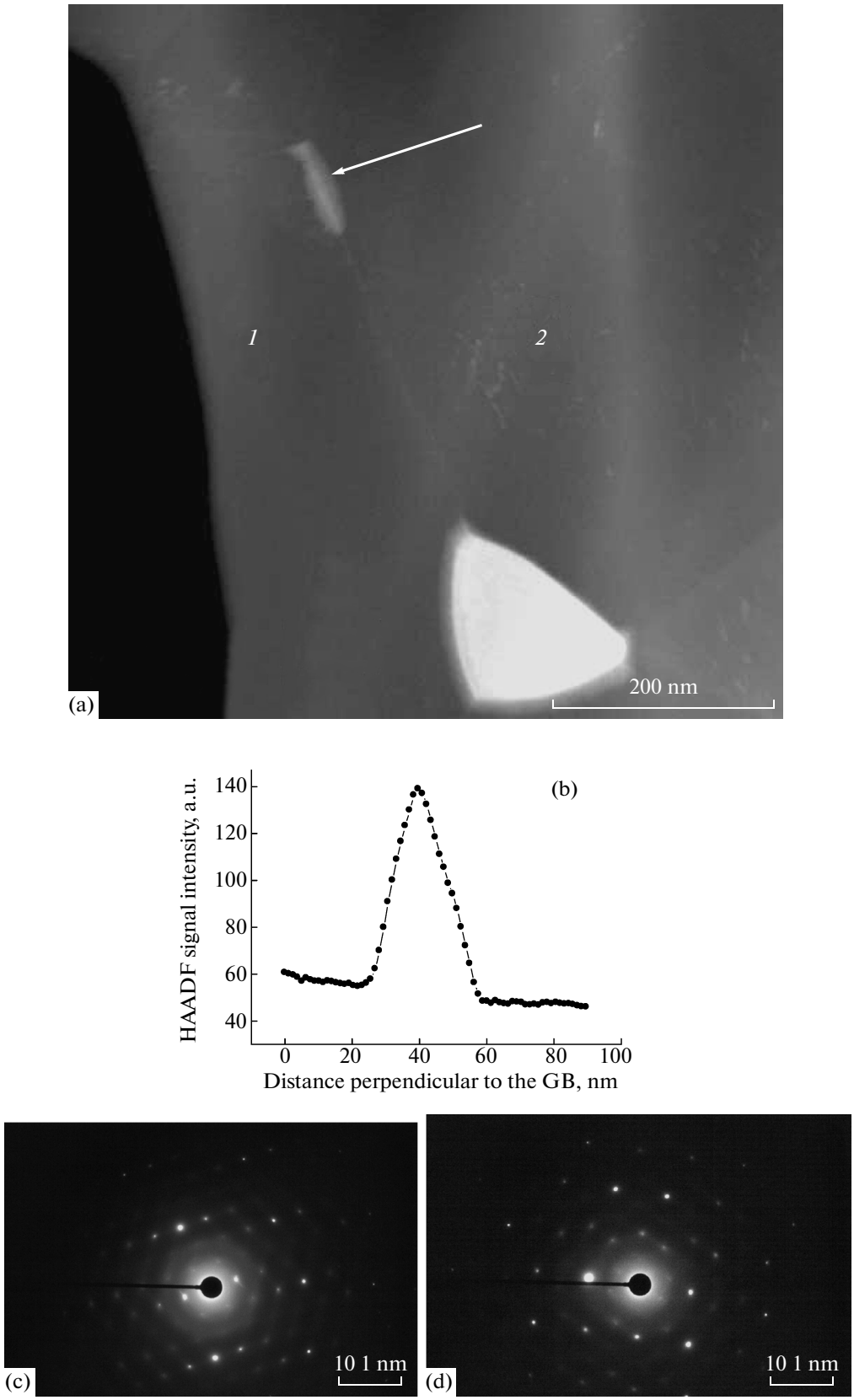

Fig. 3. Complete wetting of the Al/Al grain boundary. (a) Image recorded using the HAADF in the Z-contrast mode (the arrow notes the position of the HAADF profile), (b) intensity of the HAADF signal along the profile perpendicular to the Al/Al GB, and (c, d) local electron diffraction patterns from left *1* and right *2* Al grains.

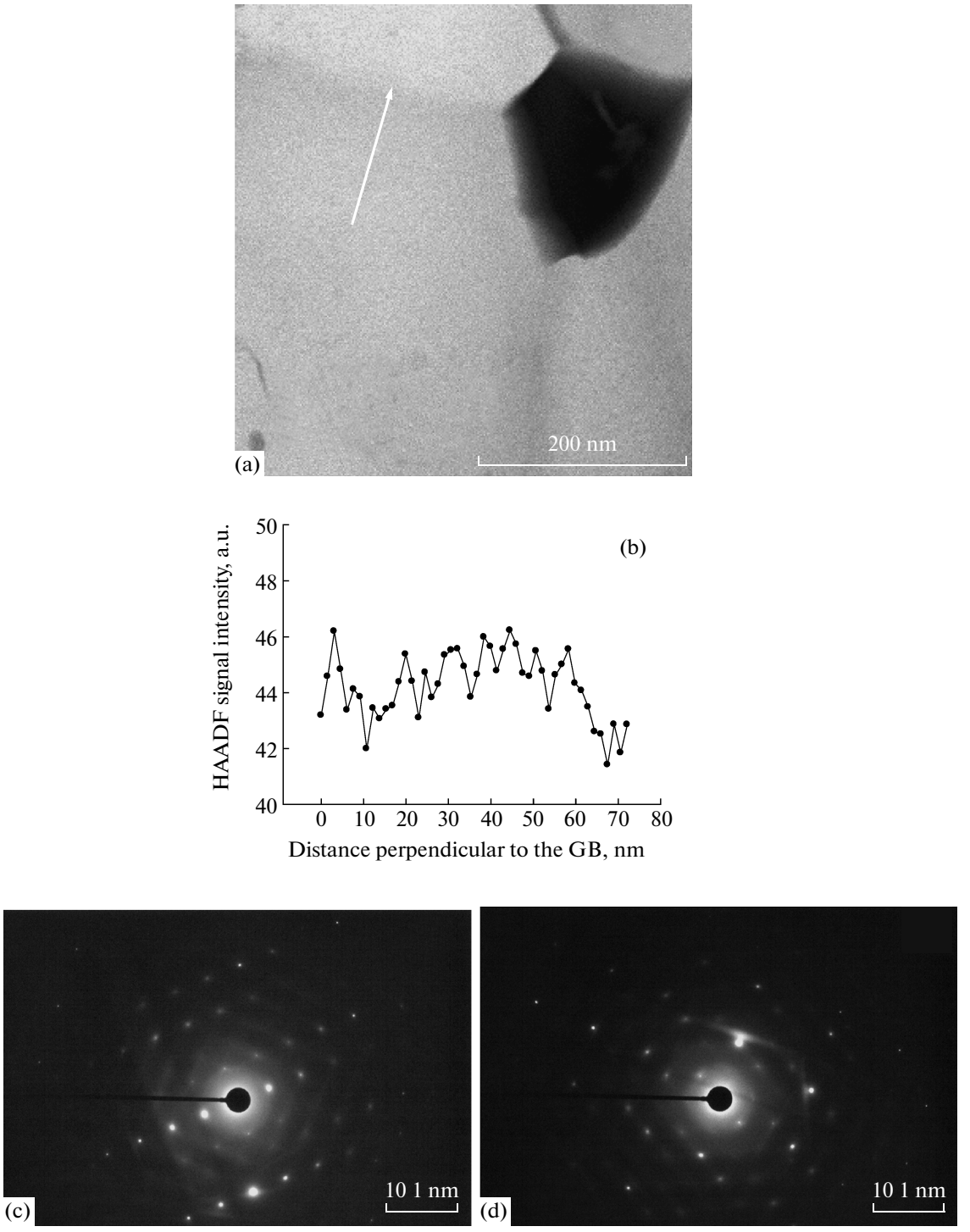

Fig. 4. Incomplete (partial) wetting of the Al/Al grain boundary. (a) Bright-field image in the STEM mode (the arrow denotes the position of the HAADF profile), (b) the intensity of the HAADF signal across the profile perpendicular to the Al/Al GB, and (c, d) local electron diffraction patterns from the upper and lower Al grains.

equichannel angular pressing or rotations of anvils under the HPT, or passages during the accumulative roll bonding).

Moreover, we can find numerous published facts which indicate that the phases in the material are different before and after the SPD [25]. Such deformation frequently leads to phase transformations such as the formation or decomposition of the supersaturated solid solution, the dissolution of phases, disordering of the ordered phases, the amorphization of crystalline

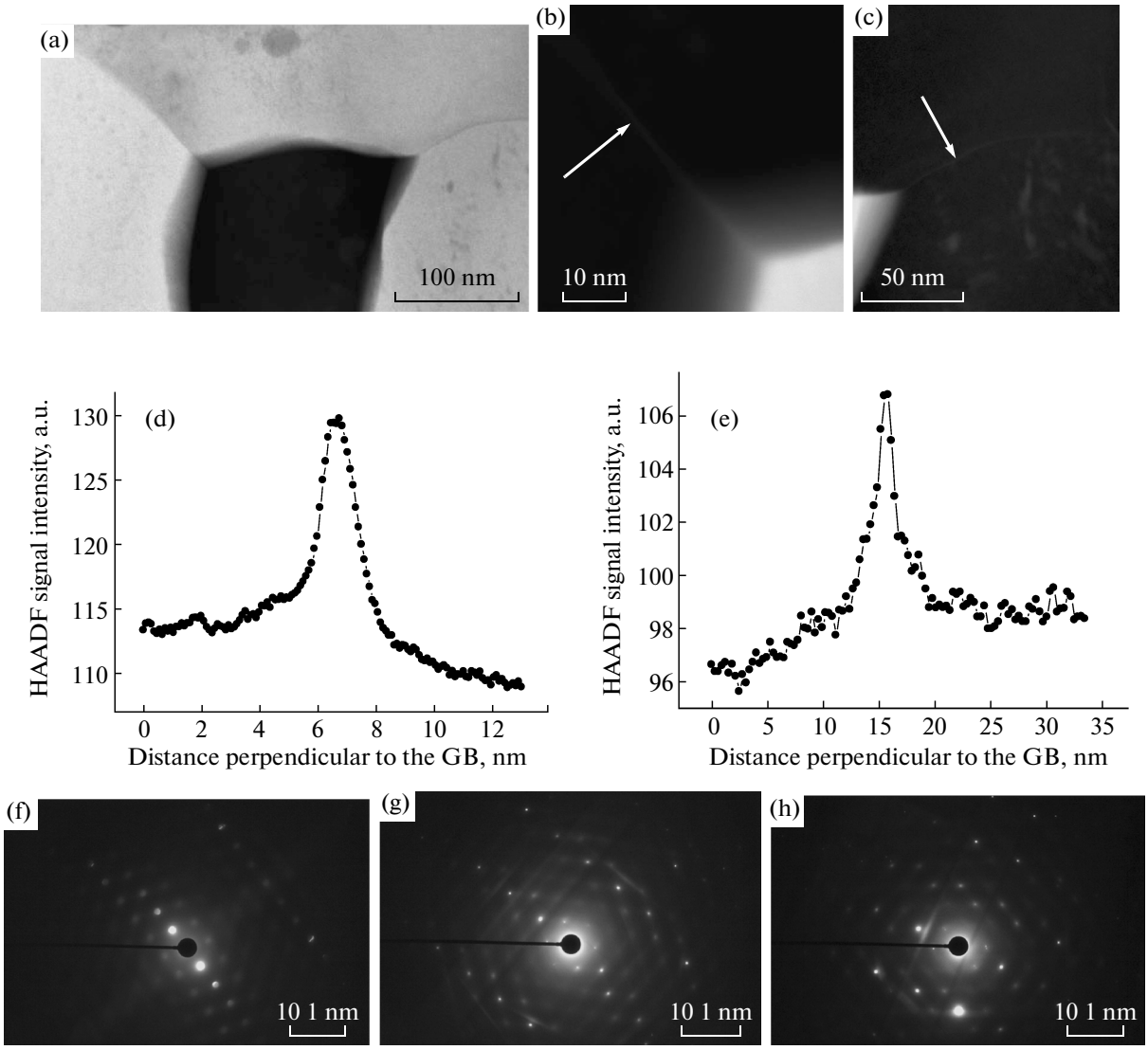

Fig. 5. Pseudopartial wetting of the Al/Al grain boundary. (a) Bright-field image in the STEM mode; (b, c) images recorded using the HAADF STEM in the *Z*-contrast mode for left and right Al/Al GBs, respectively (arrows denote the position of the HAADF profiles); (d, e) intensities of the HAADF signal from the left and right Al/Al GBs, respectively; and (f, g, h) local electron microdiffraction patterns from the left, middle, and right Al grains.

phases, and the synthesis of low-temperature and high-temperature allotropic polymorphs or high-pressure phases as well as nanocrystallization in the amorphous matrix [25]. Room-temperature SPD usually leads to very rapid phase transformations. This fact can be easily understood taking into account the high density of forming defects similarly to that occurring with an increase in temperature. On the contrary, the elevated pressure leads to a decrease in diffusivity and/or GB mobility [26, 27]. In other words, grains are refined in the material after the SPD, but and the phases are formed, which could form after prolonged annealing at certain temperature T_{eff} with subsequent quenching. It is not surprising that the SPD can lead not only to bulk, but also to GB phase transformations.

Unfortunately, we observed only the initial (before the HPT) and final (after it) GB states in our experiments. In addition, these are other boundaries because of the large structural changes. Therefore, it is impossible to judge on the order of the observed GB transitions—first or second—from our data. More precise experiments with a small step strain steps are necessary for this purpose.

It was shown by the authors of [2, 10] that the IW $\leftrightarrow$ CW direct transition can perform in two stages IW $\leftrightarrow$ PPW $\leftrightarrow$ CW (see Fig. 1) if the corresponding Hamaker constant changes the sign from positive to negative. It is always positive for aluminum: $A = 0.56 \pm 0.02 \times 10^{-21}$ J (solid–melt–vacuum) [28]. The Hamaker constant of low-melting metals with a noncubic lattice depends on indices of the

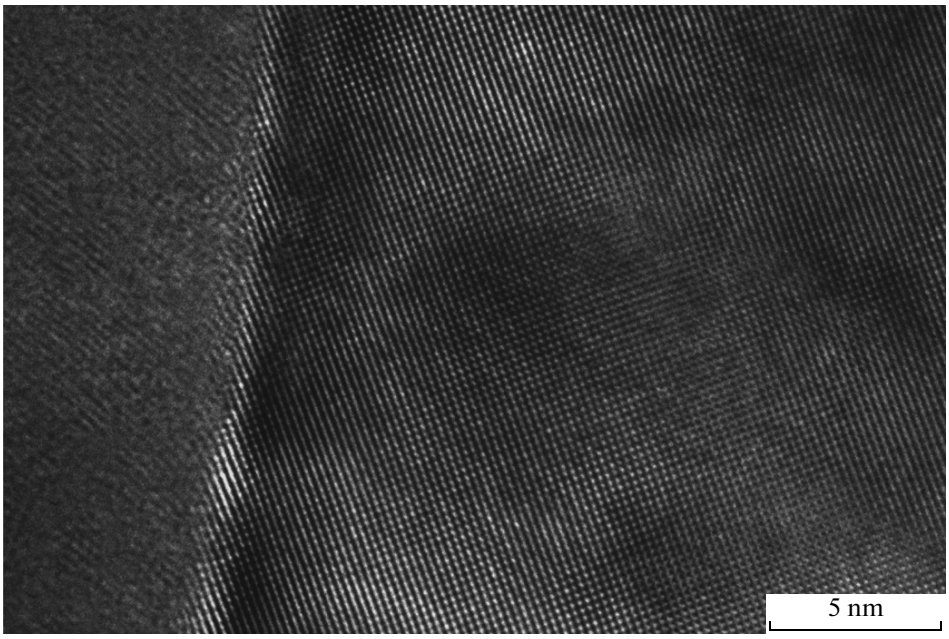

Fig. 6. Micrograph of one pseudopartially wetted Al/Al GB recorded with the help of high-resolution electron microscopy.

plane outgoing to the surface and can change the sign to negative.

The authors of [29] modified the well-known Lifshits and coauthors equation [30] for the calculation of the dependence of A on the orientation of the surface for noncubic metals:

$$A = \frac{\hbar}{16\pi^2}\int_0^{\infty} d\xi \int_{-\pi}^{+\pi} \frac{d\vartheta}{2\pi}\left[\frac{\sqrt{\varepsilon_{xx}\varepsilon'_{yy}(\vartheta)} - \varepsilon_c}{\sqrt{\varepsilon_{xx}\varepsilon'_{yy}(\vartheta)} + \varepsilon_c}\right]\frac{(1-\varepsilon_c)}{(1+\varepsilon_c)}, \quad (2)$$

where $\hbar$ is the Plank constant, ϑ is the rotation angle around axis x, ε are the components of the permittivity tensor, and ξ is the Matsubara frequency [29].

Their calculations resulted in negative values of the Hamaker constant, which differ for various crystallographic faces. For example, for planes (001) for gallium ($A = -3.0 \pm 0.02 \times 10^{-21}$ J) and β-Sn ($A = -0.45 \pm 0.1 \times 10^{-21}$ J), they were more negative than for phases (010) ($A = -2.5 \pm 0.02 \times 10^{-21}$ and $-0.38 \pm 0.1 \times 10^{-21}$ J, respectively) [28, 29]. Although the authors did not calculate the Hamaker constant for zinc, its properties from this viewpoint are comparable with properties of gallium, cadmium, and β-Sn.

However, the situation is somewhat different in our case than in [29], where constants A are determined for the solid/liquid/gas configuration; in our experiments we deal with a peculiar "sandwich" in which continuous aluminum is arranged from above and at the bottom, while a thin zinc-rich layer is arranged between them. However, the strongly positive Hamaker constant for Al, as well as a probably negative one for Zn, can form the conditions necessary for the PPW of the Al/Al GB with solid zinc.

In addition, since A for noncubic metals strongly depends on the crystallographic plane, we can expect the difference in PPW for GBs with various misorientations and inclinations [31]. Thus, varying the latter, we could perform the "fine tuning" of the Hamaker constant. This tuning was performed for wetting hexane on water by adding salt brine [2], which led to the change from direct IW ↔ CW transformation to the IW ↔ PPW ↔ CW transformation (see scheme in Fig. 1g). This occurs because constant A changes the sign in the CEP point (Fig. 1g) [32], the occurrence of which was predicted in [33]. The sequence of described transitions was observed for the first time in a mixture of alkanes and water [2].

Thus, PPW is very important from the viewpoint of technology. A high room-temperature ductility of ultrafine-grained Al–Zn alloys opens the way for the development of new light materials [23]. Thin interfacial layers-rich with cobalt between tungsten carbide grains ensures simultaneously high strength and ductility of WC–Co alloys [34]. Neodymium layers several nanometers thick between the grains of the $Nd_2Fe_{14}B$ phase ensure the unique magnetic properties of Nd–Fe–B alloys for permanent magnets [35].

CONCLUSIONS

(i) Severe plastic deformation of Al–Zn alloys by high-pressure torsion leads to the formation of three various classes of Al/Al GBs wetted by the zinc-rich solid phase, namely, completely, incompletely and pseudopartially wetted.

(ii) Completely wetted Al/Al GBs are covered with a layer of a zinc-rich solid phase more than 30 nm

thick. Incompletely wetted Al/Al GBs lie between the particles of the zinc-rich solid phase with a contact angle >60° and contain no measurable zinc concentration.

(iii) Pseudopartially wetted Al/Al GBs are similar to incompletely wetted ones: they are also arranged between the particles of the zinc-rich solid phase with a contact angle >60°. However, they contain a thin layer of the zinc-rich phase with a uniform thickness of 2–4 nm. Its presence causes an unusually high ductility of Al–Zn alloys after high-pressure torsion.

ACKNOWLEDGMENTS

This study was supported by the Ministry of Education and Science of the Russian Federation in the scope of the Program for Increasing the Competitiveness of the National University of Science and Technology "MISiS", by the grant 14.A12.31.0001 and (RZV) through the Russian Program 5-100-2020 at Research Laboratory for Mechanics of New Nanomaterials, St Petersburg State Polytechnical University; by the Allianz Indusrie Forschung, project FE.5150.0028.4067; by the Karsruhe Nano Micro Facility; by the Russian Foundation for Basic Research, project nos. 13-08-90422 and 14-03-31510; and by the Ukrainian State Fund for Fundamental Research, project F53/112-2013.

REFERENCES

1. Luo, J., *Crit. Rev. Solid State Mater. Sci.*, 2007, vol. 32, no. 1, p. 67.
2. Rafaï, S., Bonn, D., Betrand, E., and Meunier, J., *Phys. Rev. Lett.*, 2004, vol. 92, no. 24, p. 245701.
3. Kaplan, W.D., Chatain, D., Wynblatt, P., and Carter, W.C., *J. Mater. Sci.*, 2013, vol. 48, no. 17, p. 5681.
4. Straumal, B.B., Rodin, A.O., Shotanov, A.E., et al., *Defect Diff. Forum*, 2013, vol. 333, p. 175.
5. Rabkin, E.I., Shvindlerman, L.S., and Straumal, B.B., *Int. J. Mod. Phys. B*, 1991, vol. 5, no. 19, p. 2989.
6. Tang, M., Carter, W.C., and Cannon, R.M., *Phys. Rev. B*, 2006, vol. 73, no. 24, p. 024102.
7. Subramaniam, A., Koch, C.T., Cannon, R.W., and Rühle, M., *Mater. Sci. Eng. A*, 2006, vol. 422, no. 1, p. 3.
8. Tang, M., Carter, W.C., and Cannon, R.W., *J. Mater. Sci.*, 2006, vol. 41, no. 23, p. 7691.
9. Gu, H., Cannon, R.W., Tanaka, I., and Rühle, M., *Mater. Sci. Eng. A*, 2006, vol. 422, no. 1, p. 51.
10. Brochard-Wyart, F., di Meglio, J.M., Quéré, D., and de Gennes, P.G., *Langmuir*, 1991, vol. 7, no. 2, p. 335.
11. de Gennes, P.G., *Rev. Mod. Phys.*, 1985, vol. 57, no. 3, p. 827.
12. Straumal, B.B., Gust, W., and Watanabe, T., *Mater. Sci. Forum*, 1999, vols. 294–296, p. 411.
13. Straumal, B.B., Gornakova, A.S., Kogtenkova, O.A., et al., *Phys. Rev. B*, 2008, vol. 78, no. 5, p. 054202.
14. Straumal, B., Rabkin, E., Lojkowski, W., et al., *Acta Mater.,* 1997, vol. 45, no. 5, p. 1931.
15. Chang, L.-S., Straumal, B.B., Rabkin, E., et al., *J. Phase Equilibria*, 1997, vol. 18, no. 2, p. 128.
16. Chang, L.-S., Rabkin, E., Straumal, B.B., et al., *Defect Diff. Forum*, 1998, vol. 156, p. 135.
17. Moon, J., Garoff, S., Wynblatt, P., and Suter, R., *Langmuir*, 2004, vol. 20, no. 2, p. 402.
18. Straumal, B., Gust, W., and Molodov, D., *Interface Sci.*, 1995, vol. 3, no. 2, p. 127.
19. López, G.A., Mittemeijer, E.J., and Straumal, B.B., *Acta Mater.*, 2004, vol. 52, no. 6, p. 4537.
20. Protasova, S.G., Kogtenkova, O.A., Straumal, B.B., et al., *J. Mater. Sci.*, 2011, vol. 46, no. 11, p. 4349.
21. Straumal, B., Valiev, R., Kogtenkova, O., et al., *Acta Mater.*, 2008, vol. 56, no. 8, p. 6123.
22. Straumal, B., Kogtenkova, O., Protasova, S., et al., *Mater. Sci. Eng. A*, 2008, vol. 495, no. 1, p. 126.
23. Valiev, R.Z., Murashkin, M.Y., Kilmametov, A., et al., *J. Mater. Sci.*, 2010, vol. 45, no. 17, p. 4718.
24. Straumal, B.B., Kogtenkova, O.A., Protasova, S.G., et al., *J. Mater. Sci.*, 2011, vol. 46, no. 11, p. 4243.
25. Sauvage, X., Quelennec, X., and Chbihi, A., *J. Phys.: Conf. Ser.*, 2010, vol. 240, p. 012003.
26. Straumal, B.B., Klinger, L.M., and Shvindlerman, L.S., *Scripta Metal,* 1983, vol. 17, no. 3, p. 275.
27. Molodov, D.A., Straumal, B.B., and Shvindlerman, L.S., *Scripta Metal*, 1984, vol. 18, no. 3, p. 207.
28. Chen, X.J., Levi, A.C., and Tosatti, E., *Surface Sci.*, 1991, vols. 251–252, p. 641.
29. dal Corso, A. and Tosatti, E., *Phys. Rev. B*, 1993, vol. 47, no. 15, p. 9742.
30. Lifshitz, E.M., *Sov. Phys. JETP*, 1956, vol. 2, no. 1, p. 73.
31. Straumal, B.B., Klinger, L.M., and Shvindlerman, L.S., *Acta. Metall.*, 1984, vol. 32, no. 9, p. 1355.
32. Shahidzadeh, N., Bonn, D., Ragil, K., Broseta, D., and Meunier, J., *Phys. Rev. Lett.*, 1998, vol. 80, no. 18, p. 3992.
33. Ragil, K., Meunier, J., Broseta, D., et al., *Phys. Rev. Lett.*, 1996, vol. 77, no. 8, p. 1532.
34. Konyashin, I., Ries, B., Lachmann, F., et al., *Int. J. Refrac. Met. Hard Mater.*, 2008, vol. 26, no. 6, p. 583.
35. Yu, L.Q., Zhong, X.L., Zhang, Y.P., et al., *J. Magn. Magn. Mater.*, 2011, vol. 323, no. 9, p. 1152.
36. *Binary Alloy Phase Diagrams*, Massalski, T.B., Ed., OH (Materials Park): ASM International, 1990, p. 238.

Translated by N. Korovin